International Journal of Heat and Fluid Flow 30 (2009) 3–19

Contents lists available at ScienceDirect

International Journal of Heat and Fluid Flow

journal homepage: www.elsevier.com/locate/ijhff

Numerical study of dispersing pollutant clouds in a built-up environment

Bing-Chen Wang [a,*], Eugene Yee [b,1], Fue-Sang Lien [c,2]

[a] Department of Mechanical and Manufacturing Engineering, University of Manitoba, 75A Chancellors Circle, Winnipeg, Manitoba, Canada R3T 5V6
[b] Defence Research and Development Canada – Suffield, P.O. Box 4000, STN Main, Medicine Hat, AB, Canada T1A 8K6
[c] Department of Mechanical and Mechatronics Engineering, University of Waterloo, Waterloo, Ontario, Canada N2L 3G1

ARTICLE INFO

Article history:
Received 19 May 2008
Received in revised form 19 September 2008
Accepted 22 September 2008
Available online 18 November 2008

Keywords:
Urban canopy
RANS
Dispersion
Concentration variance model
Rough-wall boundary-layer
Bluff body

ABSTRACT

In this paper, we study numerically the dispersion of a passive scalar released from an instantaneous point source in a built-up (urban) environment using a Reynolds-averaged Navier–Stokes method. A nonlinear k–ϵ turbulence model [Speziale, C.G., 1987. On nonlinear k–l and k–ϵ models of turbulence. J. Fluid Mech., 178, 459–475] was used for the closure of the mean momentum equations. A tensor diffusivity model [Yoshizawa, A., 1985. Statistical analysis of the anisotropy of scalar diffusion in turbulent shear flows. Phys. Fluids, 28, 3226–3231] was used for closure of the scalar transport equations. The concentration variance was also calculated from its transport equation, for which new values of Yoshizawa's closure coefficients are used, in order to account for the instantaneous tracer release and the complex geometry. A new dissipation length-scale model, required for the modelling of the dissipation rate of concentration variance, is also proposed. The numerical results for the flow, the pollutant concentration and the concentration variance, are compared with experimental data. This data was obtained from a water-channel simulation of a full-scale field experiment of tracer dispersion through a large array of building-like obstacles known as the Mock Urban Setting Trial (MUST).

1. Introduction

The environmental and toxicological impact arising from the dispersion of contaminants released into the urban environment, where the population density is high, has become an increasingly important problem. A number of recent papers have described the measurement of urban flow and pollutant dispersion in field experiments. Large-scale urban field studies in the United States have included the URBAN 2000 meteorological and tracer field campaign conducted in Salt Lake City, Utah in October 2000 (Allwine et al., 2002), the Mock Urban Setting Trial (MUST) (Biltoft, 2001; Yee and Biltoft, 2004) conducted at US Army Dugway Proving Ground in northwestern Utah in September 2001, the Joint Urban 2003 Experiment conducted in Oklahoma City, Oklahoma (Allwine et al., 2004; Flaherty et al., 2007), and the Urban Dispersion Program (UDP) conducted in New York City, New York over the period from 2004 to 2007 (Allwine et al., 2007). Important urban field studies have been conducted in Europe such as the Dispersion of Air Pollution and its Penetration into the Local Environment (DAPPLE) which investigated the characteristics of flow in a street canyon intersection in London, UK (Arnold et al., 2004) and the Basel Urban Boundary-Layer Experiment (BUBBLE) which measured the flow of the wind through and above a homogeneous urban area (Rotach et al., 2004).

Modelling of the pollutant dispersion in an urban area has been the subject of much recent effort. To this purpose, computational fluid dynamics (CFD) has been applied to the problem of urban dispersion. There are essentially two major approaches that have been used for the numerical modelling of urban dispersion using CFD; namely, the Reynolds-averaged Navier–Stokes (RANS) and large-eddy simulation (LES) approaches. The application of CFD to pollutant dispersion in the urban environment using either RANS or LES include Baik and Kim (1999), Kim and Baik (1999), Liu and Barth (2002), Camelli et al. (2005), Coirier et al. (2005), Hsieh et al. (2007) and Milliez and Carissimo (2007). All these studies, with the exception of Hsieh et al. (2007), have focussed primarily on the prediction of the mean pollutant concentration. However, with the availability of measurements of concentration fluctuations in plumes and clouds dispersing in an urban environment (and particularly in the MUST field experiment as described by Yee and Biltoft (2004)), there have been efforts undertaken recently to model also the concentration variance field in the dispersing plume or cloud. These efforts include Andronopoulos et al. (2002), Hsieh et al. (2007), Wang et al. (2007) and Milliez and Carissimo (2008).

* Corresponding author. Tel.: +1 (204) 474 9305; fax: +1 (204) 275 7507.
E-mail addresses: bc_wang@umanitoba.ca (B.-C. Wang), eugene.yee@drdc-rddc.gc.ca (E. Yee), fslien@mecheng1.uwaterloo.ca (F.-S. Lien).
[1] Tel.: +1 (403) 544 4791; fax: +1 (403) 544 3388.
[2] Tel.: +1 (519) 888 4567x36528; fax: +1 (519) 888 6197.

0142-727X/$ - see front matter © 2008 Elsevier Inc. All rights reserved.
doi:10.1016/j.ijheatfluidflow.2008.09.008

Nomenclature

c	instantaneous concentration
$\bar{c}$	mean concentration
$\overline{c'^2}$	concentration variance
C_μ	closure constant for eddy-viscosity
$C_{\epsilon 1}$, $C_{\epsilon 2}$	closure constants (Eq. (4))
C_s	source concentration
C_{s1}, C_{s2}	closure constants (Eq. (10))
$C_{\chi_{21}}$, $C_{\chi_{22}}$	closure constants (Eq. (20))
$C_{\tau 1}$, $C_{\tau 2}$, $C_{\tau 3}$	closure constants (Eq. (8))
d_0	diameter of the point source
D	molecular diffusivity
D_{jk}	tensor diffusivity
D_n	normalized total dosage ($\equiv \mathscr{D}/C_s$)
$\mathscr{D}$	total dosage
H	height of the obstacle (in the vertical direction)
k	turbulent kinetic energy (TKE)
l_x, l_y	streamwise and spanwise spacing between obstacles
L	length of the obstacle (in the streamwise direction)
$\bar{p}$	kinematic mean pressure
P_k	rate of TKE production
Re	Reynolds number
S	source strength of the tracer
t	time
t_d	dissipation time scale
t_s	characteristic time scale ($\equiv L/U_b$)
$\bar{u}_i$	mean velocity component in the i-th coordinate direction
U_b	free stream velocity
v_n	normalized mean spanwise velocity ($\equiv \bar{v}/U_b$)
W	width of the obstacle (in the spanwise direction)
x, y, z	streamwise, spanwise and vertical coordinates
$\bar{x}_c$, $\bar{y}_c$, $\bar{z}_c$	x, y and z coordinates of the cloud centroid
δ	boundary-layer thickness
δ_{ij}	Kronecker delta
ϵ	rate of TKE dissipation
ϵ_c	rate of concentration variance dissipation
Λ_0	initial cloud size
Λ_d	dissipation length-scale of a cloud
Λ_I	integral length-scale of turbulence
ν_t	kinematic eddy-viscosity
σ_x, σ_y, σ_z	cloud spreads in the x-, y- and z-directions
σ_k, σ_ϵ	closure constants (Eqs. (3) and (4))
$\overline{(\cdot)}$	ensemble-averaged quantity

1.1. Laboratory and numerical simulations of MUST

The MUST field experiment, conducted at US Army Dugway Proving Ground in September 2001, was designed to provide measurements of fluctuating concentrations in a plume or cloud dispersing through a large array of building-like obstacles. After the completion of the original MUST field experiment, a series of scaled laboratory experiments were conducted. A wind-tunnel simulation of the MUST array at a 1:50 scale was undertaken by the Defence Science and Technology Organisation of Australia in the 1.5-MW boundary-layer wind-tunnel at Monash University, Victoria, Australia (Gailis and Hill, 2006; Yee et al., 2006). A water-channel simulation of the MUST array at 1:205 scale was conducted in the water-channel facility at Coanda R&D Corporation, Burnaby, British Columbia, Canada in a study sponsored by Defence Research and Development Canada (Yee et al., 2006; Hilderman and Chong, 2007).

The series of MUST experiments provided high-quality data sets, that have been used for validation of numerical models for urban flow and pollutant dispersion. Towards this objective, the full-scale MUST field experiments have been used to evaluate the empirical urban dispersion models in Hazard Prediction Assessment Capability (HPAC) (Warner et al., 2006). Camelli et al. (2004, 2005) and Milliez and Carissimo (2007, 2008) simulated the MUST field trials using the LES and RANS methodologies, respectively. Hsieh et al. (2007) and Wang et al. (2007) simulated the MUST water-channel experiments using both the RANS and unsteady RANS (URANS) approaches.

A unique feature of the MUST water-channel experiment was the performance of a sufficient number of controlled repeat releases to enable the behavior of concentration fluctuations in clouds dispersing in a built-up environment to be studied. The current series of tracer experiments involving instantaneous clouds provide an extensive new data set that can be used to evaluate the predictive accuracy of numerical models for the transient release of passive scalars in a built-up environment. To date, numerical studies of dispersion in the MUST array (Camelli et al., 2004, 2005; Milliez and Carissimo, 2007, 2008) have focused primarily on the simulation of dispersing plumes resulting from the continuous release of a tracer for the full-scale field experiment. The preliminary results reported in Hsieh et al. (2007) is the first numerical study that has modelled the dispersion of a passive scalar from both continuous and instantaneous releases in an idealized obstacle array (including comparisons with experimental data obtained from the water-channel simulation of the MUST array).

This paper focusses on a detailed numerical study of cloud transport and dispersion within and above an urban canopy (MUST array). This study was undertaken using a RANS model incorporating more sophisticated turbulence closure schemes than those that have been used previously. Indeed, previous numerical studies of the flow and dispersion in the MUST array (Milliez and Carissimo, 2007, 2008; Hsieh et al., 2007; Wang et al., 2007) have used only a simple eddy-viscosity model (Boussinesq eddy-viscosity approximation) for the Reynolds stress tensor required for closure of the mean momentum equation and a simple isotropic eddy-diffusivity model (gradient diffusion hypothesis) for the turbulent scalar flux vector required for closure of the transport equations for the mean concentration and for the concentration variance.

There are many nonlinear k–ϵ turbulence models for the Reynolds stress tensor and these have been reviewed by Wilcox (1998). In this paper, we consider only the nonlinear k–ϵ turbulence model proposed by Speziale (1987) for closure of the mean momentum equations. Similarly, there are a variety of tensor diffusivity scalar flux models available in the literature, such as those developed by Yoshizawa (1985, 1988), Rogers et al. (1989), Rubinstein and Barton (1991), Wikström et al. (2000), Younis et al. (2005) and So et al. (2004). Moreover, recent reviews of these types of models can be found in So and Speziale (1999), Hanjalić (2002) and Younis et al. (2005). In this study, we focus on a critical assessment of the performance of only one of these tensor diffusivity scalar flux models for the prediction of urban dispersion; namely, the tensor diffusivity scalar flux model of Yoshizawa (1985).

It is challenging to implement a tensor diffusivity scalar flux model for the numerical simulation of the concentration statistics in an instantaneous cloud dispersing in a built-up environment for

a number of reasons. Firstly, investigations of the application of tensor diffusivity scalar flux models for urban dispersion are non-existent. Secondly, tensor diffusivity scalar flux models have been designed primarily for closure of the transport equation for the mean concentration. The efficacy of these models for closure of the transport equation for the concentration variance is unknown. Thirdly, most of the tensor diffusivity models (including that of Yoshizawa (1985)) have been designed for distributed scalars (e.g., temperature field in a non-buoyant flow). The predictive accuracy of these models for an instantaneous release of a passive scalar from a localized source will need to be carefully assessed. Finally, the closure coefficients for conventional tensor diffusivity models have been primarily calibrated against simple (canonical) test cases. How well these anisotropic scalar flux models work for the highly disturbed flows in an urban canopy (e.g., MUST obstacle array) will need to be investigated.

This paper is organized in the following manner. In Section 2, the water-channel experiment conducted to study flow and dispersion in the MUST obstacle array will be briefly introduced. In Section 3, the numerical methodology and turbulence stress and scalar flux models will be described, and a new dissipation length-scale model required for the closure of the concentration variance transport equation will be proposed. In Section 4, the proposed modelling approach is validated by comparing the model predictions with the experimental results. Finally, in Section 5, the major conclusions will be summarized.

2. Water-channel simulations of MUST

The water-channel experiment for MUST is fully described in Hilderman and Chong (2007), and only the important details of the experiment will be summarized here. The experiment was conducted in the boundary-layer water-channel facility at Coanda R&D Corporation (Burnaby, British Columbia, Canada). This water-channel has a working test section of length 10 m, width 1.5 m and height 0.9 m.

The water-channel experiment simulated a deep neutrally stratified atmospheric boundary-layer flow over an array of three-dimensional (3-D) building-like obstacles used for MUST. The MUST obstacle array was simulated at a scale of 1:205, so each sharp-edged obstacle in the array had a length (L) of 11.8 mm, width (W) of 59.4 mm and height (H) of 12.4 mm. A total of 120 obstacles was placed in an aligned array of 12 rows of 10 obstacles (see Fig. 1 for a photograph of the scaled-down version of the MUST array and Figs. 2a and b for a description of its geometry). The streamwise and spanwise spacing between obstacles was $l_x = 5.33L = 62.9$ mm and $l_y = 3.26L = 38.5$ mm, respectively.

The fully developed flow upstream of the MUST array was created in the channel using a combination of a "turbulence grid" of square bars and a sawtooth fence placed at the channel inlet. The free stream velocity (velocity at the top of the boundary-layer with depth $\delta = 275$ mm) is $U_b = 0.38$ m s^{-1}. The Reynolds number of the flow in the water-channel simulation was approximately $Re_H = 4700$ (based on U_b and H). In our analysis of the experimental results and numerical simulations, flow quantities were non-dimensionalized using U_b and L (implying that the time scale for non-dimensionalization was $t_s = L/U_b = 0.031$ s). Fig. 2 illustrates the geometry of the MUST array and shows the coordinate system that was used for the numerical simulations. All streamwise (or x) distances are referenced relative to the upstream edge of the first row of obstacles at $x/L = 0$, and the origin of the coordinate system in the spanwise (or y) direction is taken to be along the centerline ($y/L = 0$) of the fifth column of obstacles in the array.

The ground-level point source for the instantaneous release was located at row 1.5 (viz., at a position halfway between the first and second rows of obstacles in the array) along the centerline of the fifth column of obstacles. The x and y coordinates of the source location are $x_s/L = 3.67$ and $y_s/L = 0$. The diameter of the point source was $d_0 = 2.8$ mm. The instantaneous point source emitted a sodium fluorescein dye tracer at a volume flow rate of 24 ml min^{-1} for a duration of 1.25 s. For each puff experiment, a series of 100 individual puffs were released and this set of realizations of cloud dispersion allowed ensemble-averaged concentration statistics (e.g., mean concentration, concentration variance) in the developing cloud to be determined. The puff-cloud passages from each replicate of the instantaneous release were sampled for 33.3 s after each initial release. This sampling duration was long enough to contain the entire passage of the cloud at any receptor location in the array.

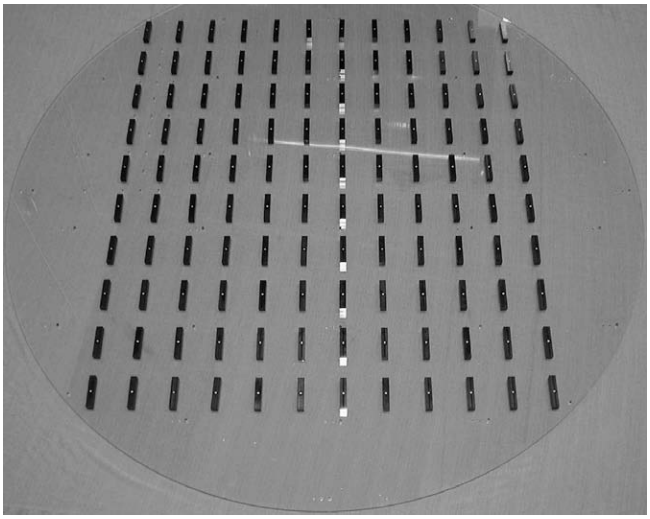

Fig. 1. MUST array in water-channel.

The velocity field was measured using a 4-beam 2-component fibre-optic laser doppler anemometer (LDA) powered by an argon-ion laser. Titanium dioxide particles were used as seed particles. The LDA data were collected over a sampling time of 500 s at each position. The data rate for the LDA measurements depended upon the flow velocity, particle seeding density, and optical properties of the lenses, but was typically 50–500 Hz.

The concentration field was measured using a laser-induced fluorescence (LIF) linescan system. The linescan LIF system allows simultaneous multi-point concentration measurements to be made along the laser beam. The fluorescent intensity of the tracer was measured using a Dalsa monochrome digital linescan CCD camera with 12-bit amplitude resolution (4096 digitization levels) at a rate of 300 Hz. Each linescan consisted of 1024 pixels, giving a spatial resolution between 0.5 and 1 mm depending on the relative position of the camera and laser line.

3. Numerical model and turbulence closure

In this section, we first describe the governing equations for the simulation of the disturbed flow within and over an idealized obstacle array and the concomitant dispersion of a tracer released into this flow. Next, the nonlinear models required to close these equations are described. In particular, we formulate a new scalar dissipation length-scale model required to close the transport equation for the concentration variance. Finally, the numerical framework used to solve the system of modelled governing equations is briefly described.

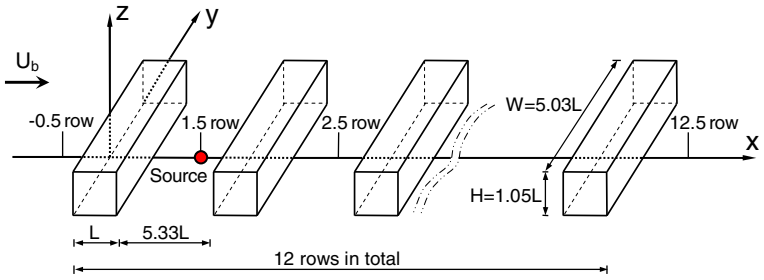

(a) Schematic of fifth column of obstacles in the MUST array

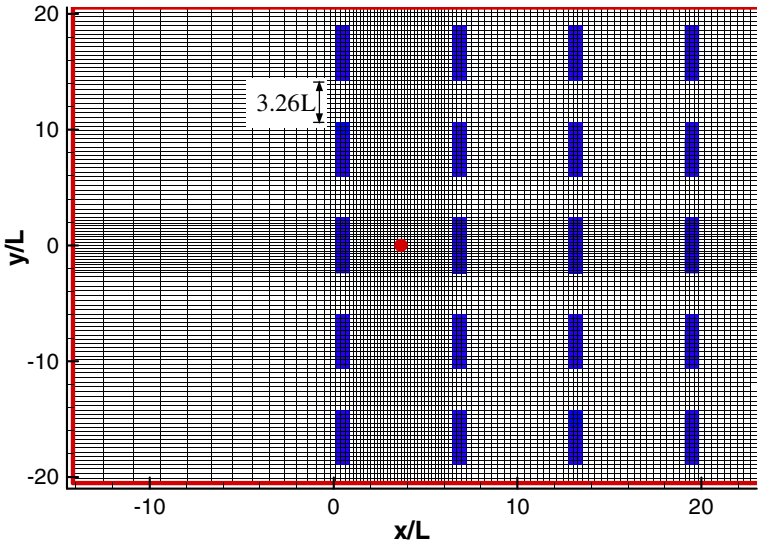

(b) A portion of the grid system (x-y view)

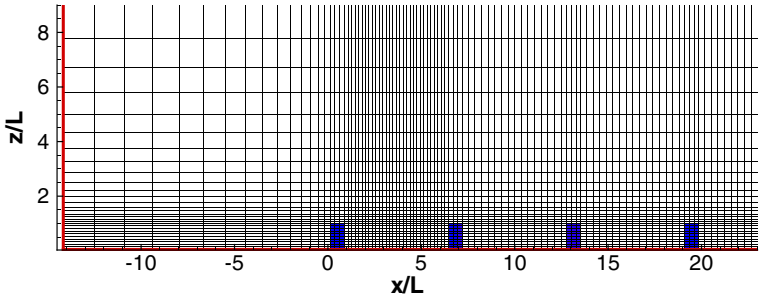

(c) A portion of the grid system (x-z view)

Fig. 2. Geometry of the obstacles and the coordinate system of the MUST array (L = 11.8 mm). The x-axis is aligned along the fifth column of obstacles in the array. The point source is located at y/L = 0 and at row 1.5 (i.e., at x/L = 3.67, or halfway between the first and second rows of obstacles in the array). The grid system shown here is for the small domain.

3.1. Governing equations

The mean flow, mean concentration and concentration variance fields are described by the conservation laws of mass and momentum and the transport equations for the mean concentration and concentration variance. In addition to these equations, the transport equations for TKE and for the rate of dissipation ϵ of TKE are also required. These governing equations for an incompressible and neutrally stratified fluid flow and a conservative passive scalar assume the following form in a Cartesian coordinate system:

$$\frac{\partial \bar{u}_i}{\partial x_i} = 0, \tag{1}$$

$$\frac{\partial \bar{u}_i}{\partial t} + \frac{\partial (\bar{u}_i \bar{u}_j)}{\partial x_j} = -\frac{\partial \bar{p}}{\partial x_i} + \frac{\partial}{\partial x_j}\left(\nu \frac{\partial \bar{u}_i}{\partial x_j}\right) - \frac{\partial \overline{u_i' u_j'}}{\partial x_j}, \tag{2}$$

$$\frac{\partial k}{\partial t} + \frac{\partial (\bar{u}_j k)}{\partial x_j} = \frac{\partial}{\partial x_j}\left[\left(\nu + \frac{\nu_t}{\sigma_k}\right)\frac{\partial k}{\partial x_j}\right] + P_k - \epsilon, \tag{3}$$

$$\frac{\partial \epsilon}{\partial t} + \frac{\partial (\bar{u}_j \epsilon)}{\partial x_j} = \frac{\partial}{\partial x_j}\left[\left(\nu + \frac{\nu_t}{\sigma_\epsilon}\right)\frac{\partial \epsilon}{\partial x_j}\right] + \frac{\epsilon}{k}(C_{\epsilon_1} P_k - C_{\epsilon_2}\epsilon), \tag{4}$$

$$\frac{\partial \bar{c}}{\partial t} + \frac{\partial (\bar{u}_j \bar{c})}{\partial x_j} = \frac{\partial}{\partial x_j}\left(D \frac{\partial \bar{c}}{\partial x_j}\right) - \frac{\partial \overline{u_j' c'}}{\partial x_j} + S, \tag{5}$$

$$\frac{\partial \overline{c'^2}}{\partial t} + \frac{\partial (\bar{u}_j \overline{c'^2})}{\partial x_j} = \frac{\partial}{\partial x_j}\left(D \frac{\partial \overline{c'^2}}{\partial x_j} - \overline{u_j' c'^2}\right) - 2\overline{u_j' c'}\frac{\partial \bar{c}}{\partial x_j} - \epsilon_c. \tag{6}$$

Here, $\bar{u}_i$ is the mean (or, ensemble-averaged) velocity in the x_i-coordinate direction, with i = 1, 2 or 3 representing the streamwise x, spanwise y or vertical z directions; $\bar{p}$ is the kinematic mean pressure; $\bar{c}$ is the mean concentration; $\overline{c'^2}$ is the concentration variance; S is the source density distribution of the scalar; D is the molecular

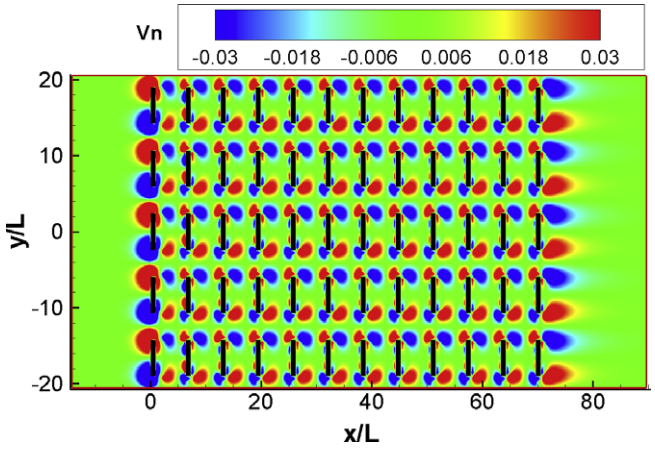

Fig. 3. Mean vortex shedding in the array visualized using isopleths of the normalized spanwise velocity $v_n \equiv \bar{v}/U_b$ obtained in a horizontal plane at height $z/H = 0.61$. This result shown here is for the small domain.

diffusivity of the scalar; ν is the kinematic viscosity of the fluid; $\nu_t \equiv C_\mu k^2/\epsilon$ is the kinematic eddy-viscosity; $\overline{u_i' u_j'}$ is the kinematic Reynolds stress tensor; $\overline{u_j' c'}$ is the turbulent flux of concentration; $\overline{u_j' c'^2}$ is the turbulent flux of concentration variance; $P_k \equiv -\overline{u_i' u_j'}\partial \bar{u}_i/\partial x_j$ is the production of TKE; and, ϵ_c is the concentration variance dissipation rate defined as

$$\epsilon_c = 2D\overline{\frac{\partial c'}{\partial x_j}\frac{\partial c'}{\partial x_j}}. \tag{7}$$

The closure constants are given as follows: $C_\mu = 0.09$, $\sigma_k = 1.0$, $\sigma_\epsilon = 1.3$, $C_{\epsilon 1} = 1.44$ and $C_{\epsilon 2} = 1.92$.

3.2. Nonlinear constitutive relations for stress and scalar flux

In order to close the governing equations, the kinematic Reynolds stresses (i.e., $\overline{u_i' u_j'}$) and turbulent fluxes of the concentration and concentration variance (i.e., $\overline{u_j' c'}$ and $\overline{u_j' c'^2}$, respectively) need to be modelled. We use an explicit algebraic nonlinear model formulation for the Reynolds stresses; namely, the quadratic model of Speziale (1987) to close the mean momentum equation:

$$\begin{aligned}\overline{u_i' u_j'} = {} & \frac{2}{3}k\delta_{ij} - \nu_t\left(\frac{\partial \bar{u}_i}{\partial x_j} + \frac{\partial \bar{u}_j}{\partial x_i}\right) \\ & + \frac{k^3}{\epsilon^2}\left[C_{\tau 1}\left(\frac{\partial \bar{u}_i}{\partial x_k}\frac{\partial \bar{u}_j}{\partial x_k}\right)^* + C_{\tau 2}\left(\frac{\partial \bar{u}_i}{\partial x_k}\frac{\partial \bar{u}_k}{\partial x_j} + \frac{\partial \bar{u}_j}{\partial x_k}\frac{\partial \bar{u}_k}{\partial x_i}\right)^*\right. \\ & \left. + C_{\tau 3}\left(\frac{\partial \bar{u}_k}{\partial x_i}\frac{\partial \bar{u}_k}{\partial x_j}\right)^*\right],\end{aligned} \tag{8}$$

where δ_{ij} is the Kronecker delta, and an asterisk indicates the deviatoric part of a tensor, i.e. $(\cdot)^*_{ij} \equiv (\cdot)_{ij} - (\cdot)_{kk}\delta_{ij}/3$. The three model coefficients appearing in this equation are: $C_{\tau 1} = 0.041$, $C_{\tau 2} = 0.014$ and $C_{\tau 3} = -0.014$.

The model of Speziale (1987) provides a nonlinear constitutive relation between the Reynolds stress tensor and the mean velocity gradients. The original model of Speziale (1987) contained the convective derivatives of the mean velocity gradients, which have been removed in the present treatment in order to improve the numerical stability (see Gatski and Speziale, 1993; Lien and Leschziner, 1994a). Because the objective of the current study is the transport and dispersion of contaminants in a built-up environment, we will simply treat Speziale's nonlinear k–ϵ model as a standard turbulence closure model and focus our attention instead on the modelling of the turbulent concentration flux and the concentration variance dissipation rate.

For the turbulent scalar fluxes, we use the tensor (anisotropic) diffusivity model of Yoshizawa (1985); namely,

$$\overline{u_j' c'} = -D_{jk}\frac{\partial \bar{c}}{\partial x_k} \quad \text{and} \quad \overline{u_j' c'^2} = -D_{jk}\frac{\partial \overline{c'^2}}{\partial x_k}, \tag{9}$$

where the tensor diffusivity D_{jk} is defined as

$$D_{jk} = C_{s1}\frac{k^2}{\epsilon}\delta_{jk} + C_{s2}\frac{k^3}{\epsilon^2}\left(\frac{\partial \bar{u}_j}{\partial x_k} + \frac{\partial \bar{u}_k}{\partial x_j}\right). \tag{10}$$

Here, C_{s1} and C_{s2} are two model coefficients. It is important to note that Yoshizawa's tensor diffusivity model has only been applied to closure of the turbulent concentration flux (first part of Eq. (9)). To the authors' knowledge, this model has never been applied to the closure of the turbulent flux of concentration variance (second part of Eq. (9)), and one of the objectives of the current work is to investigate the applicability of this model for the representation of $\overline{u_j' c'^2}$.

The two model coefficient C_{s1} and C_{s2} were calibrated for Eq. (5) and not for Eq. (6), using simple test cases for isotropic turbulence and thin shear flows. As such, the values of these two coefficients might not be treated as universal, especially when this model is used for predicting the concentration variance in a cloud dispersing in an urban environment.

3.3. Concentration variance dissipation model

In order to close Eq. (6), the concentration variance dissipation rate ϵ_c needs to be modelled. One approach to this problem is to solve a transport equation for ϵ_c. This approach involves several higher-order correlation terms that need to be modelled (e.g., terms that involve a triple correlation of the gradients of the fluctuating velocity and scalar). The modelled transport equation for ϵ_c then contains six closure coefficients (for detailed description of the modelled ϵ_c-transport equation, see Yoshizawa (1988) and So and Speziale (1999)). Unfortunately, there is little experience concerning this approach and its applicability to cloud dispersion in an urban canopy is questionable.

In view of this, it is simpler to try to formulate an appropriate algebraic model for ϵ_c. In this approach, ϵ_c is modelled simply as (Warhaft and Lumley, 1978)

$$\epsilon_c = C_{\chi_1}\frac{1}{t_d}\overline{c'^2} = C_{\chi_1}\frac{\epsilon}{k}\overline{c'^2}, \tag{11}$$

in which the dissipation time scale (t_d) is proportional to the integral turbulence time scale $t_I = k/\epsilon$ (with an associated integral turbulence length-scale given by $\Lambda_I = k^{3/2}/\epsilon$). The value of the closure constant C_{χ_1} varies in the literature (Warhaft, 2000). This constant is usually set to 2, following the suggestion of Béguier et al. (1978). In this paper, we refer to this conventional model as Model-1.

It is useful to consider an alternative model for ϵ_c. To this end, consider a formulation for the dissipation time scale t_d in terms of a characteristic velocity for the turbulence (which can be chosen as $k^{1/2}$) and a scalar dissipation length-scale Λ_d:

$$\epsilon_c = C_{\chi_2}\frac{k^{1/2}}{\Lambda_d}\overline{c'^2}, \tag{12}$$

where C_{χ_2} is a closure constant. The key issue in this model is the determination of the value of Λ_d. Note that for the conventional Model-1, $\Lambda_d = \Lambda_I$. Recently, Hsieh et al. (2007) proposed a simple model for the dissipation length-scale, which evaluates Λ_d using a local scale for the dispersing cloud taken as the geometric mean of the cloud spreads in the three coordinate directions:

$$\Lambda_{d3D} = \Lambda_{d3D}(t) = \left(\sigma_x(t)\sigma_y(t)\sigma_z(t)\right)^{1/3}, \tag{13}$$

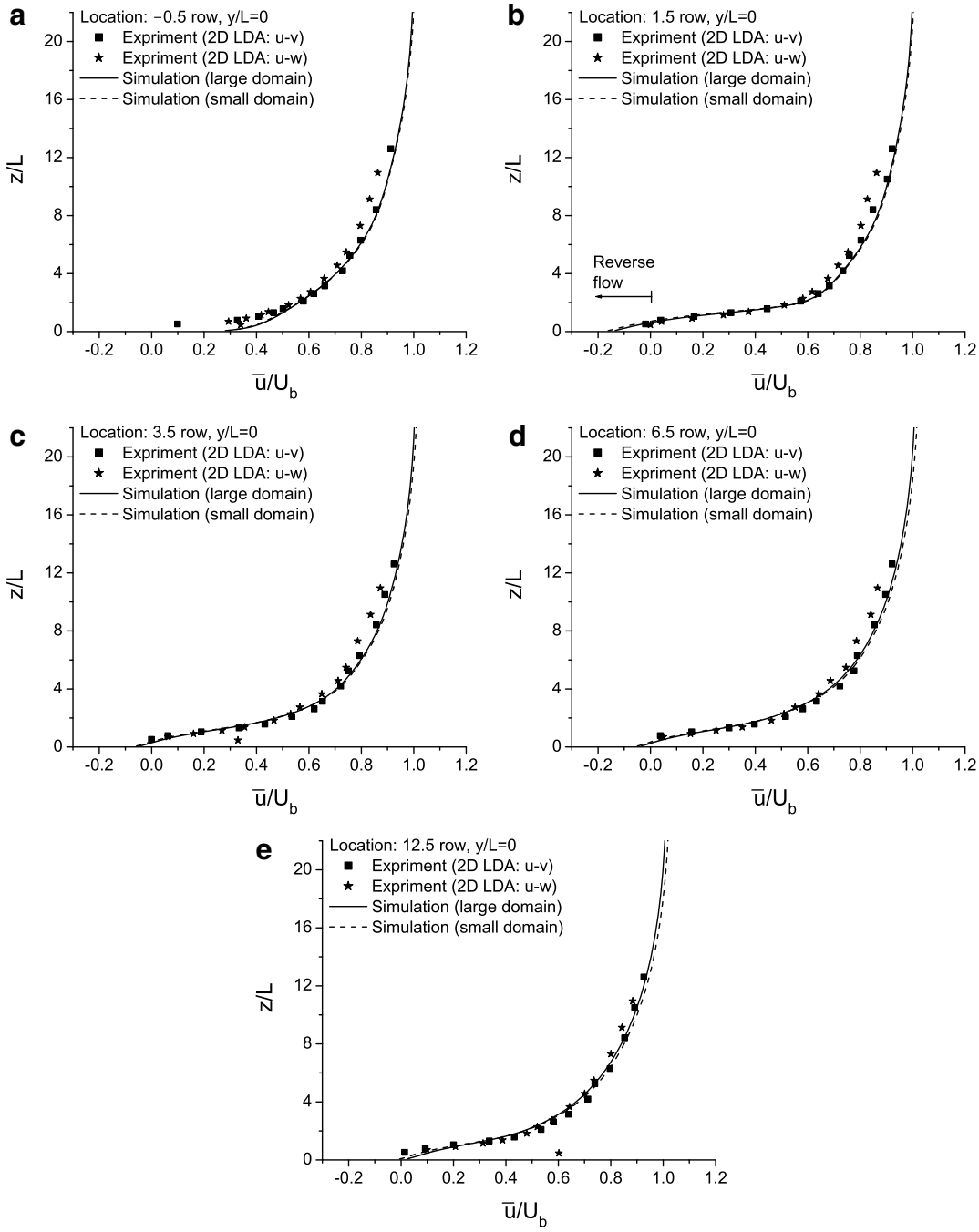

Fig. 4. Vertical profiles of the normalized mean streamwise velocity, $\bar{u}/U_b$, obtained at five x-locations along $y/L = 0$.

where $\sigma_x(t)$, $\sigma_y(t)$ and $\sigma_z(t)$ are the cloud spreads in the x-, y-, and z-directions, respectively, at (travel) time t after the initial release. The streamwise cloud spread is defined as

$$\sigma_x(t) = \left(\frac{\int\int\int (x - \bar{x}_c)^2 \bar{c}(x,y,z,t) dxdydz}{\int\int\int \bar{c}(x,y,z,t) dxdydz} \right)^{1/2}, \tag{14}$$

with the streamwise position of the cloud centroid determined from

$$\bar{x}_c = \bar{x}_c(t) = \frac{\int\int\int x\bar{c}(x,y,z,t) dxdydz}{\int\int\int \bar{c}(x,y,z,t) dxdydz}. \tag{15}$$

The cloud spread in the other two coordinate directions are defined in an analogous manner.

A modification to the dissipation length-scale model used by Hsieh et al. (2007) is proposed. Experience with the use of this model seems to suggest that Λ_d given by Eq. (13) can significantly over-estimate the scalar dissipation length-scale, owing to enhanced streamwise dispersion resulting from the strong shear flow that exists at or near the top of an urban canopy. This over-estimation of Λ_d leads to an under-estimation in the scalar dissipation rate ϵ_c. In particular, Fig. 6 shows the time evolution of the cloud spreads in the three coordinate directions, for one of our simulations of the MUST case. This figure shows that the x-wise growth of the cloud occurs much more quickly than the cloud growth in the other two coordinate directions. This is the result of the shear-enhanced streamwise dispersion in the obstacle array. The non-uniformity of the mean velocity field here distorts the shape

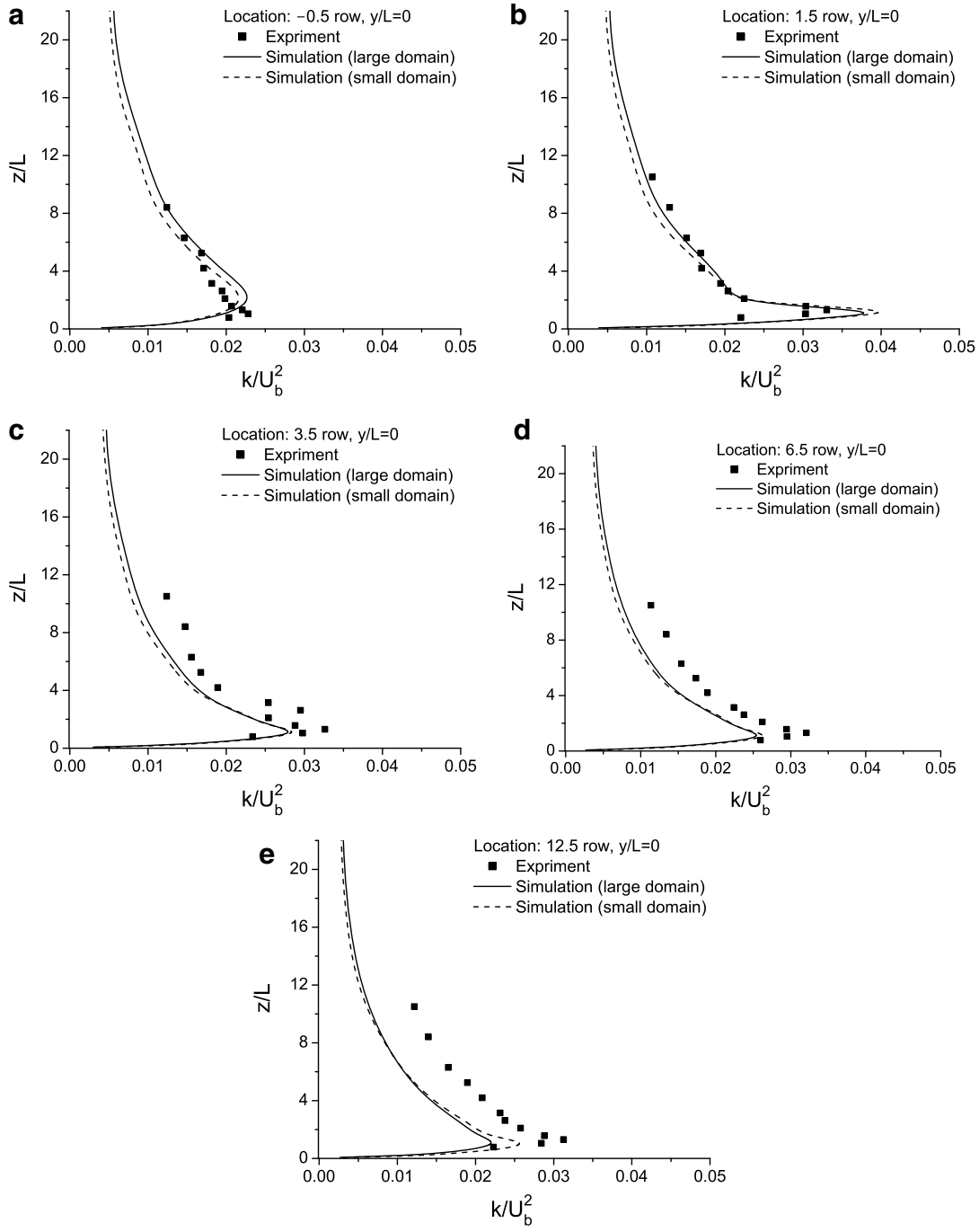

Fig. 5. Vertical profiles of the normalized turbulent kinetic energy, k/U_b^2, obtained at five x-locations along $y/L = 0$.

of the cloud by greatly stretching and elongating it in the streamwise direction, relative to the other two coordinate directions.

In view of this, we modified Eq. (13) so that only the cloud spreads in the cross-stream directions are used in the determination of Λ_d, so

$$\Lambda_{d2D} = \Lambda_{d2D}(x,t) = (\sigma_y^{2D}(x,t)\sigma_z^{2D}(x,t))^{1/2}, \tag{16}$$

where the "cloud spreads" $\sigma_y^{2D}(x,t)$ and $\sigma_z^{2D}(x,t)$ are evaluated locally in the vertical y–z (or, cross-stream) plane. The "cloud spread" $\sigma_y^{2D}(x,t)$ in the y-direction is determined as

$$\sigma_y^{2D}(x,t) = \left(\frac{\int\int (y-\bar{y}_c^{2D})^2 \bar{c}(x,y,z,t)dydz}{\int\int \bar{c}(x,y,z,t)dydz}\right)^{1/2}, \tag{17}$$

with the y-location of the cloud centroid in the local y–z plane evaluated from

$$\bar{y}_c^{2D} = \bar{y}_c^{2D}(x,t) = \frac{\int\int y\bar{c}(x,y,z,t)dydz}{\int\int \bar{c}(x,y,z,t)dydz}. \tag{18}$$

The expression for $\sigma_z^{2D}(x,t)$ is defined in an analogous manner to Eq. (17).

Following from these arguments, our model for the concentration variance dissipation rate follows from the general form of Eq. (12):

$$\epsilon_c = \frac{k^{1/2}}{\Lambda_d}\overline{c'^2}, \tag{19}$$

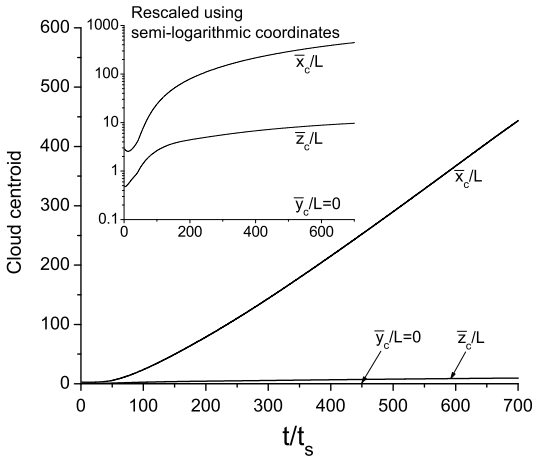

(a) Cloud centroids

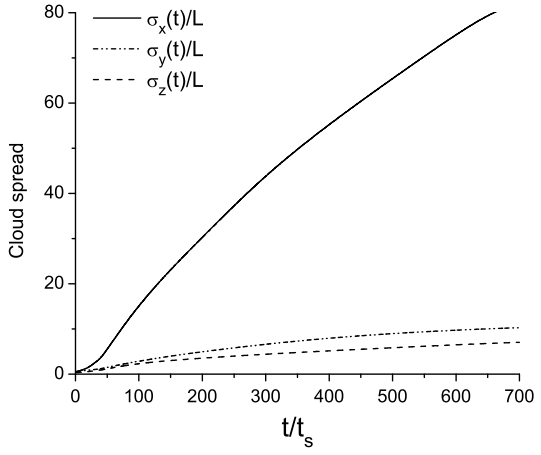

(b) Cloud spreads

Fig. 6. Temporal evolution of (a) cloud centroid and (b) cloud spread in the three coordinate directions. The result shown here is for the large domain. Here, $t_s \equiv L/U_b$ is a characteristic time scale for the flow in the obstacle array.

with the closure constant C_{χ_2} absorbed into the definition of Λ_d and with the following formulation proposed for modelling Λ_d:

$$\Lambda_d = \Lambda_d(x,t) = \max\left[\Lambda_0, \min\left(\frac{\Lambda_{d2D}}{C_{\chi_{21}}}, \frac{\Lambda_{I2D}}{C_{\chi_{22}}}\right)\right]. \tag{20}$$

Here, $C_{\chi_{21}} = C_{\chi_{22}} = 1.5$ are two model constants, and Λ_0 is the initial cloud size taken as $\Lambda_0 = d_0/2$ (for this case). The model constants $C_{\chi_{21}}$ and $C_{\chi_{22}}$ were fixed to values that provided good quantitative agreement with the MUST dispersion data; and, more specifically, with the observed decay of the concentration variance along the cloud centerline. This model ensures that the scalar dissipation length-scale Λ_d is greater than or equal to the initial source size, and the imposition of this lower limit also prevents any potential numerical instability from occurring (viz., if $\Lambda_d \to 0$) in Eq. (19). Furthermore, in Eq. (20), Λ_{I2D}[3] is the integral length-scale of turbulence averaged over a vertical cross-section of the cloud, viz.

$$\Lambda_{I2D} = \Lambda_{I2D}(x,t) = \frac{\int\int \Lambda_I \bar{c}(x,y,z,t)dydz}{\int\int \bar{c}(x,y,z,t)dydz}. \tag{21}$$

This new length-scale model (i.e., Eq. (20)) also ensures that when the cloud-averaged scalar length-scale Λ_{d2D} exceeds the cloud-averaged integral turbulence length-scale Λ_{I2D}, then it is the latter scale which defines Λ_d. At this stage, the cloud has reached the regime of homogeneous turbulent mixing. The proposed model represented by Eqs. (19) and (20) will be referred to henceforth as Model-2.

3.4. Numerical framework

The numerical simulations were performed with two in-house computer codes: the flow code urbanSTREAM and the dispersion code urbanEU, both of which employ a fully collocated storage arrangement for all transported properties (viz., mean velocity vector, pressure, k and ϵ in urbanSTREAM and $\bar{c}$ and $\overline{c'^2}$ in urbanEU). In each code, the partial differential equations which model the unsteady, three-dimensional flow field in urbanSTREAM and the developing mean concentration and concentration variance fields in urbanEU were developed in a general non-orthogonal (curvilinear) coordinate system and solved using a finite volume method (Yee et al., 2007).

The flow solver used in urbanSTREAM is based on the numerical algorithms described by Lien and Leschziner (1994b). Advective finite volume face fluxes are approximated using a total-variation-diminishing (TVD) variant (Lien and Leschziner, 1994c) of the higher-order quadratic upwind interpolation for the convective kinematics (QUICK) scheme developed by Leonard (1979). The physical diffusive finite volume face fluxes are approximated using a conventional second-order central difference scheme. The SIMPLE algorithm was used for the pressure correction (Patankar, 1980). Here, mass continuity is enforced by solving a pressure correction equation which, as part of the iterative sequence, steers the pressure toward a state in which all mass residuals in the finite volumes are negligibly small. In conjunction with the collocated grid used here, this method is known to provoke checkerboard oscillations in the pressure field as discussed in Patankar (1980), reflecting a state of pressure-velocity decoupling. To avoid this, the method proposed by Rhie and Chow (1983) is used to nonlinearly interpolate the finite volume face velocities from the nodal values at the centers of the finite volumes.

Within the iterative scheme, the transport equations for $\bar{u}_i$ ($i = 1,2,3$), k and ϵ and the pressure correction equation are solved sequentially and iterated to convergence, defined by reference to L1-residual norms for the mass and momentum equations. Here, the L1-residual norm is defined as the sum of absolute residuals over all grid points in the computational domain. The L1-residual norms for the mass and momentum components were normalized by the mass and momentum fluxes at the inflow plane. A convergent solution was assumed after each normalized L1-residual norm decreased below 0.00005. The discretized equations in urbanSTREAM are solved using an iterative method, known as the strongly implicit procedure (SIP) proposed by Stone (1968) which uses an incomplete lower–upper (LU) decomposition. The converged mean velocity and turbulence fields from urbanSTREAM were used to "drive" urbanEU, and the discretized transport equations for the mean concentration and concentration variance were solved using the SIP method. Convergence was declared when the ratio of the L1-residual norm for the discretized equation in the current iteration to that for the first iteration is smaller than a prescribed tolerance (typically 10^{-7}).

At the inflow boundary plane, Dirichlet boundary conditions were imposed for the mean velocity and turbulent kinetic energy using the measured distributions for these quantities obtained

[3] The integral lengthscale $\Lambda_I(x,y,z)$ is a function of x, y and z in the highly disturbed and strongly inhomogeneous flow in an urban canopy. Because $\Lambda_{d2D}(x)$ in Eq. (20) involves an average over the cloud in a cross-stream plane, it is more appropriate to compare the magnitude of $\Lambda_{d2D}(x)$ with the magnitude of the turbulence integral length-scale averaged also over the cloud in the same cross-stream plane (viz., with $\Lambda_{I2D}(x)$).

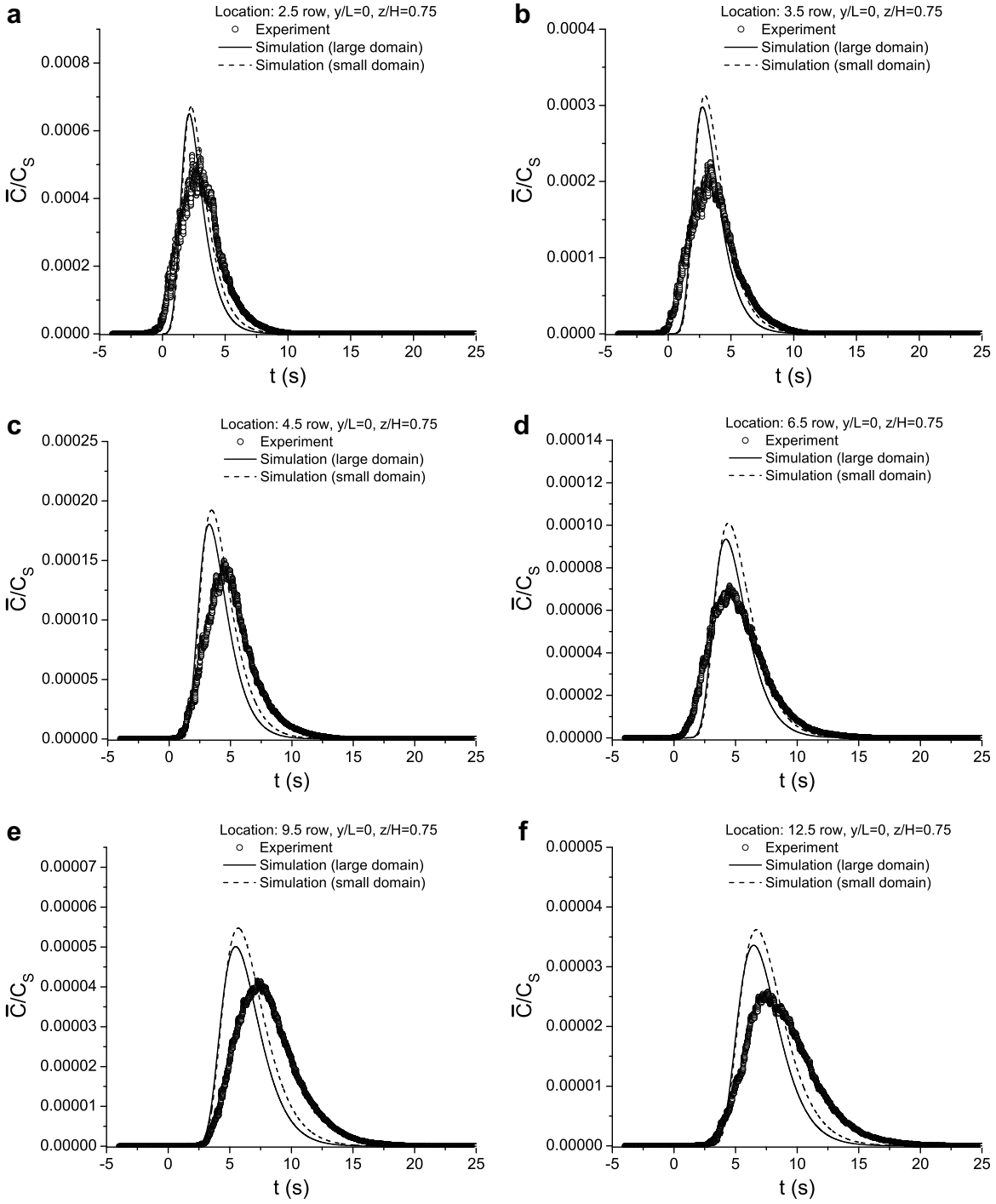

Fig. 7. Time history of the normalized mean concentration, $\bar{c}/C_s$, in the cloud obtained at six x-locations along $y/L = 0$ and within the canopy at the height $z/H = 0.75$.

from the experiment.[4] Far downstream, at the outflow boundary plane, the flow was assumed to reach a fully developed state in which no changes occur in the flow direction. Hence, at the outflow boundary, the horizontal gradients of all flow variables are assumed to be zero. At the upper boundary, we used free-slip conditions for all flow variables. A periodic boundary-condition was applied in the spanwise direction for all flow variables across the vertical boundary planes that define the lateral boundaries for the computational domain. At all solid boundaries (ground, obstacle walls and roofs) in the computational domain, standard wall functions (Launder and Spalding, 1974) are used for mean velocities and turbulence quantities. For the mean concentration and concentration variance, at the computational flow domain boundaries and at all solid boundaries in the computational domain, zero-flux Neumann conditions were applied.

In this study, two different grids and computational domains were used in order to determine if the computed solutions for

[4] The vertical profiles of the mean velocity and turbulent kinetic energy in the inlet boundary plane upwind of the MUST obstacle array were measured by Hilderman and Chong (2007), who used this data to demonstrate the horizontal homogeneity of the velocity statistics in the upstream approach flow.

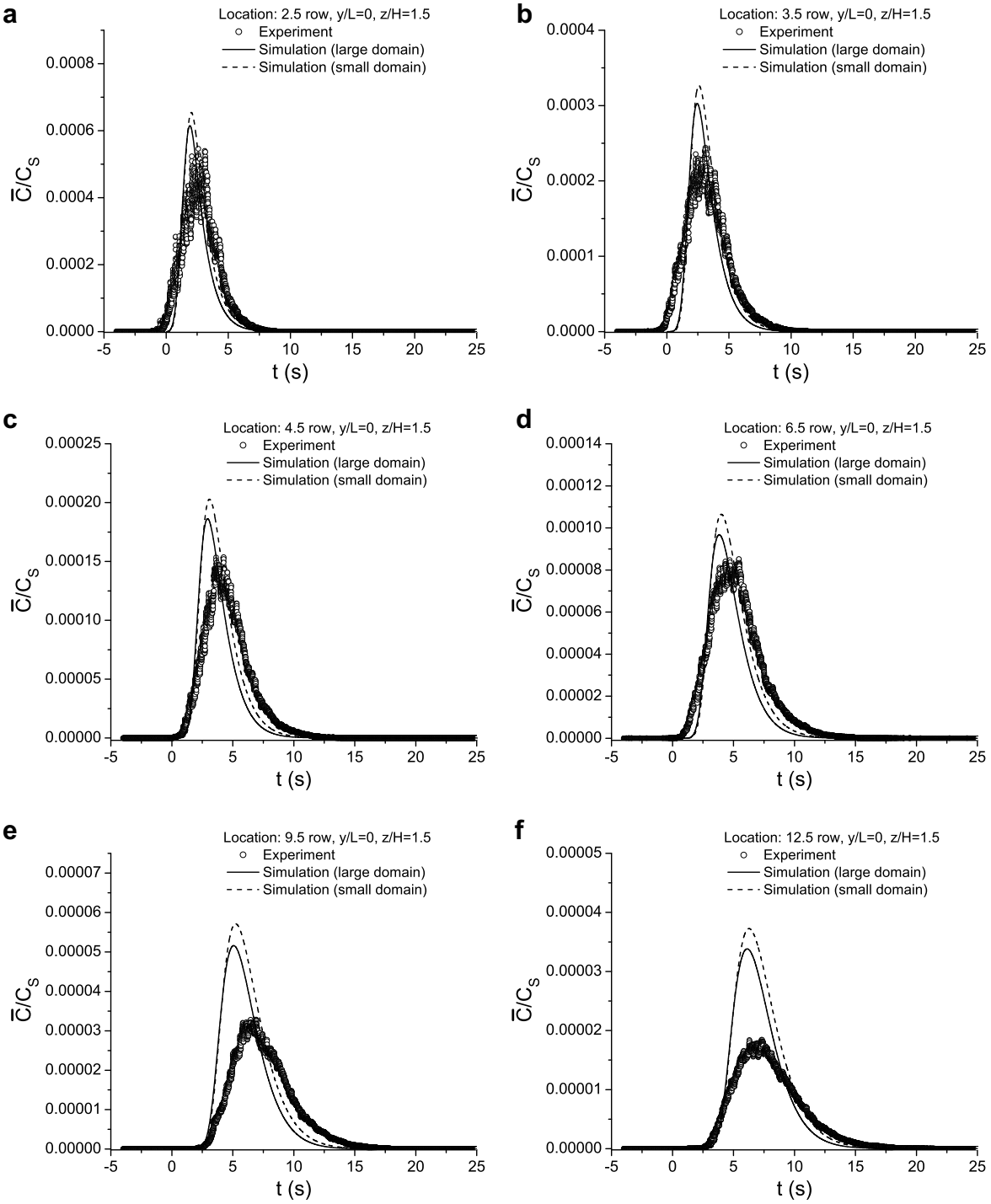

Fig. 8. Time history of the normalized mean concentration, $\bar{c}/C_s$, in the cloud obtained at six x-locations along $y/L = 0$ and above the canopy at the height $z/H = 1.5$.

the velocity and concentration fields were grid-independent. These two grids were also used to investigate the sensitivity of predicted concentration and concentration variance fields to how well the grid can resolve the spatial extent (size) of the localized source used in the experiments. For these purposes, the size for the large and small computational domains used in this study were, respectively, as follows: $685.6L \times 41.5L \times 60L$ and $105.6L \times 41.5L \times 30L$, with $224 \times 53 \times 30$ and $185 \times 83 \times 42$ control volumes (in the streamwise, spanwise, and wall-normal directions, respectively). An upstream fetch of $15L$ (distance between the inflow plane and the windward face of the first row of obstacles) was used for both the large and small computational domains. The major difference between these two computational domains was in the extent of the downstream fetch between the last row of obstacles and the outflow plane. Furthermore, the grid system for the small computational domain is finer (i.e., provides a higher-resolution grid) than that for the large computational domain.

Both the large and small computational domains include 12 rows and 5 central columns of MUST obstacles. As shown later, including only 5 central columns of the MUST obstacle array (and imposing periodicity in the mean velocity and turbulence fields in the spanwise direction) for the simulations was sufficient

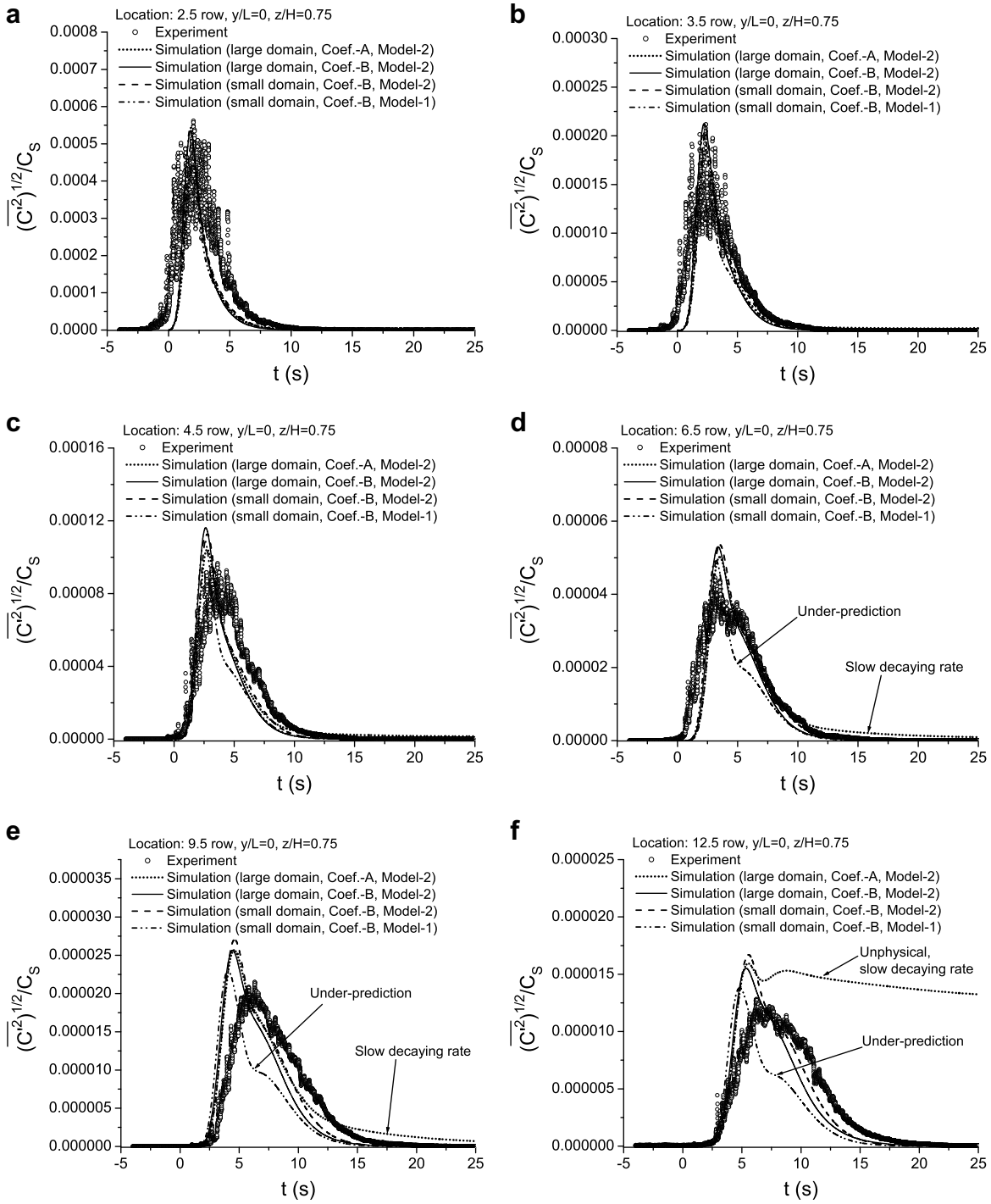

Fig. 9. Time history of the normalized concentration standard deviation, $(\overline{c'^2})^{1/2}/C_s$, in the cloud obtained at six x-locations along $y/L = 0$ and within the canopy at the height $z/H = 0.75$.

to provide good predictions of the flow and concentration quantities. As depicted in Figs. 2b and c, the grid lines were preferentially concentrated near the location of the source (which was at $x/L = 3.67$ and $y/L = 0$) and in the vicinity of every solid surface (e.g., walls, rooftops, ground) where the gradients in the flow properties are expected to be the greatest. The spacing between the grid lines was gently stretched with increasing distance from the solid surfaces.

In order to predict the mean concentration and concentration variance of the puff-cloud as it evolves within and above the MUST array, a total time of 25 s was simulated using URANS with a temporal resolution of 0.05 s per time step.

4. Results

In this section, numerical predictions of the flow in terms of the mean velocity and turbulence kinetic energy will be compared with experimental values at five different streamwise locations. Dispersion in terms of the mean concentration and concentration variance will be compared to the corresponding experimental data

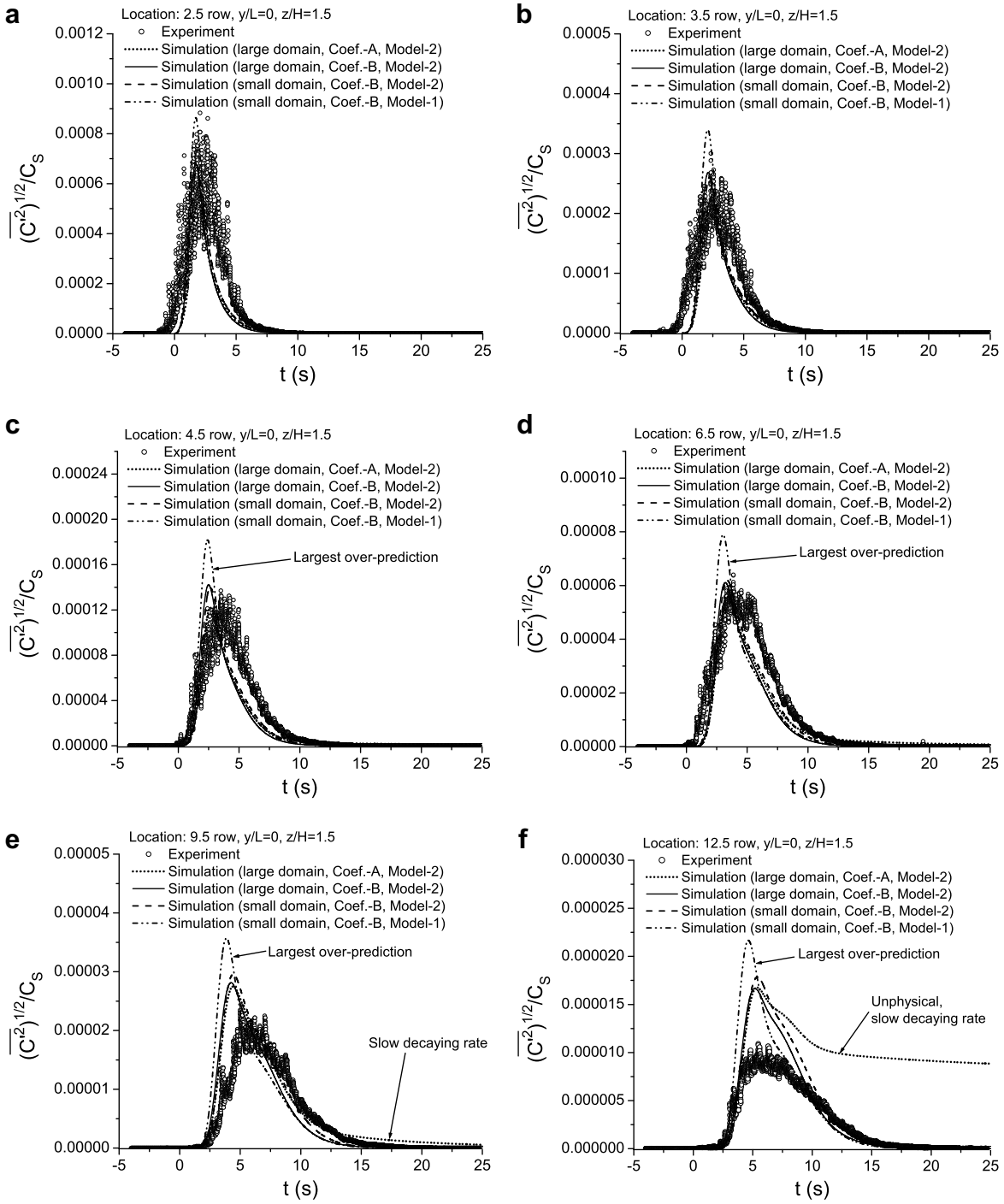

Fig. 10. Time history of the normalized concentration standard deviation, $(\overline{c'^2})^{1/2}/C_s$, in the cloud obtained at six x-locations along $y/L = 0$ and above the canopy at the height $z/H = 1.5$.

at six streamwise locations both within and above the obstacle array.

4.1. Velocity statistics

This subsection assesses the ability of urbanSTREAM concerning the simulation of the disturbed wind flow through the MUST obstacle array. To this end, we compare RANS-predicted streamwise mean velocity and turbulent kinetic energy with the corresponding measured quantities.

Fig. 3 displays isopleths of the normalized mean spanwise velocity $v_n \equiv \bar{v}/U_b$ in a horizontal plane through the MUST array at the height $z/H = 0.61$. This figure shows the result for the simulation undertaken on the small computational domain, which provides a qualitative visualization of the complex topology of vortex shedding in the obstacle array predicted using the RANS approach. It can be seen that as the flow passes by an obstacle in the array, symmetrical mean vortical structures are generated, and these vortical structures are much larger at the front and rear edges of the array than inside the array where the size of these flow structures

are inhibited due to the presence of the neighboring obstacles. A careful examination of the topology of the mean flow patterns displayed in Fig. 3 suggests that the mean velocity field within the second urban canyon (between second and third rows of obstacles) is "typical" of its neighbors. This implies that in the MUST array interior, a streamwise periodic boundary-condition could have been imposed to model the flow in a unit cell of a single representative obstacle and the corresponding street canyon. In consequence, in the MUST obstacle array, the model predicts that the mean flow within the array adjusts to the canopy within a distance of about 7.33L.

Fig. 4 exhibits vertical profiles of the normalized mean streamwise velocity, $\bar{u}/U_b$ at five streamwise locations along the centerline of the 5th column of obstacles ($y/L = 0$). Experimental measurements for $\bar{u}$ are shown for both configurations used in the experiment (namely, the u–v and u–w configurations used by the 2-component LDA system). Agreement of the predictions provided by the RANS model for both the small and large domains is very good at almost all the streamwise locations. The two flow domains which use two different grids provide virtually identical predictions for $\bar{u}/U_b$, implying negligible domain size and grid sensitivity (for the purposes of this study) in the predictions of the mean streamwise velocity.

In the impact region upstream of the windward face of the MUST obstacle array at $x/L = -2.67$ (or, row −0.5 – see Fig. 2), the measurement and the prediction of $\bar{u}$ do not show any reversal in the mean flow close to the ground, but the RANS model overpredicts $\bar{u}$ for $z/H \lesssim 1$. At $x/L = 3.67$ (row 1.5) in the adjustment region, the model prediction captures the very strong shear layer that forms immediately downstream of the leeward (rear) face of an obstacle in the first row, whose signature is seen in the inflection point in $\bar{u}(z)$ at or near the obstacle height H. Furthermore, the magnitude of the reverse flow in the first spanwise-oriented street canyon below $z/H \approx 1/2$ is correctly predicted by the model. At $x/L = 16.33$ (row 3.5) and 35.33 (row 6.5) in the equilibrium region where the mean flow has adjusted to the urban canopy and reached streamwise equilibrium (viz., the mean streamwise velocity field is fully developed), the vertical profiles of $\bar{u}$ are almost identical to each other. This feature appears in both the measurements and model predictions. Finally, at $x/L = 73.3$ (row 12.5) in the exit region of the array directly downstream of the last row of obstacles, the predicted mean streamwise velocity is in good conformance with the measurements. The reduction in the mean shear at or near $z = H$ is predicted correctly at this x-location as $\bar{u}$ begins the recovery towards the far upwind undisturbed reference state.

Fig. 5 exhibits the vertical profiles of the turbulent kinetic energy, k, at the same x-locations as the mean streamwise velocity shown in Fig. 4. At $x/L = -2.67$ (row −0.5) in the impact region, the predicted levels of turbulence energy are good. More specifically, the increase in k above the height H as an obstacle in the first row of the array is approached is predicted quite well, although prediction of the location of maximum k appears to be too far away from the ground at this x-location. At $x = 3.67$ (row 1.5), the position of the prominent "nose" in the k profile lying at or just above the top of the first row of obstacles is correctly reproduced by the model prediction. Comparing k at $x/L = 16.33$ (row 3.5) and 35.33 (row 6.5), it is seen that the peak value of k, lying at the center of the shear or mixing layer near the top of the canopy, attenuates downstream. This feature in the TKE is captured correctly by the model predictions, although the peak values of k at these two x-locations are slightly under-predicted. Although the prediction of the TKE profile at $x/L = 73.3$ (row 12.5 in the exit region) is very similar in shape to the measured profile and the position of the maximum TKE is fairly well predicted, the level of turbulence energy is under-predicted by the model at this location.

4.2. Concentration statistics

The model predictions of the location of the cloud centroid, $(\bar{x}_c, \bar{y}_c, \bar{z}_c)$, and the cloud spread, $(\sigma_x, \sigma_y, \sigma_z)$, in the three coordinate directions (normalized by L) for the instantaneous release (whose location is indicated in Fig. 2) as a function of the normalized travel time, t/t_s, are shown in Fig. 6. The most striking feature in Fig. 6 is that the streamwise cloud spread, σ_x, occurs significantly faster (by orders of magnitude) than the cloud spreads in the two directions normal to the x-direction. This implies that shape of the mean cloud is highly anisotropic (hence, highly distorted) as it disperses within and above the obstacle array. As shown in Fig. 4, the magnitude of the very strong wind shear that develops at or near canopy height H and the enhanced vertical turbulent diffusion in the z-direction owing to the increased production of TKE in this shear layer (see Fig. 5), results in a shear-enhanced streamwise dispersion in the cloud.

Predictions of the time history of the ensemble-averaged normalized concentration profiles, $\bar{c}/C_s$, along the centerline of the mean cloud at $y/L = 0$ at six downstream distances at two different heights within and above the canopy ($z/H = 0.75$ and 1.5) are exhibited, respectively, in Figs. 7 and 8. Here, C_s is the source concentration (viz., concentration of tracer released from the source). Experimental measurements of $\bar{c}/C_s$ have been superimposed in the figures for comparison with the URANS model predictions. It is noted that the shapes of the mean concentration time profiles are generally predicted well by the model. The model predictions and the measurements both show that these profiles are skewed to the right with the leading edge of the profile rising more rapidly than the trailing edge, the latter of which is seen to exhibit a long tail region of decay. In general, the arrival time of the cloud (i.e., the delay before the cloud reaches the receptor location) is predicted quite well by the model, although the time at which the cloud reaches its maximum value is under-predicted slightly by the model. Furthermore, the value of the peak mean concentration at each receptor location is over-predicted by the model, whereas the "duration" (i.e., delay between the arrival and departure time) of the cloud is slightly under-predicted. The predictions for $\bar{c}$ exhibit a relatively small sensitivity to the use of the small and large domains with the fine- and coarse-grid resolutions — certainly, the differences in the predicted $\bar{c}$ arising from the sizes of the two flow domains and their concomitant discretizations are less than about 10%.

Figs. 9 and 10 compare predictions of the time history of the normalized concentration standard deviation, $(\overline{c'^2})^{1/2}/C_s$, with

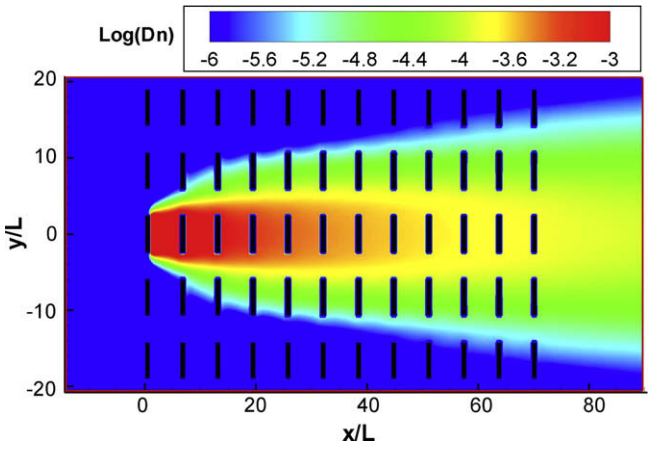

Fig. 11. Normalized total dosage $D_n \equiv \mathscr{D}/C_s$ isopleths displayed on a logarithmic scale obtained in a horizontal plane at the height $z/H = 0.61$. The result shown here is for the small domain.

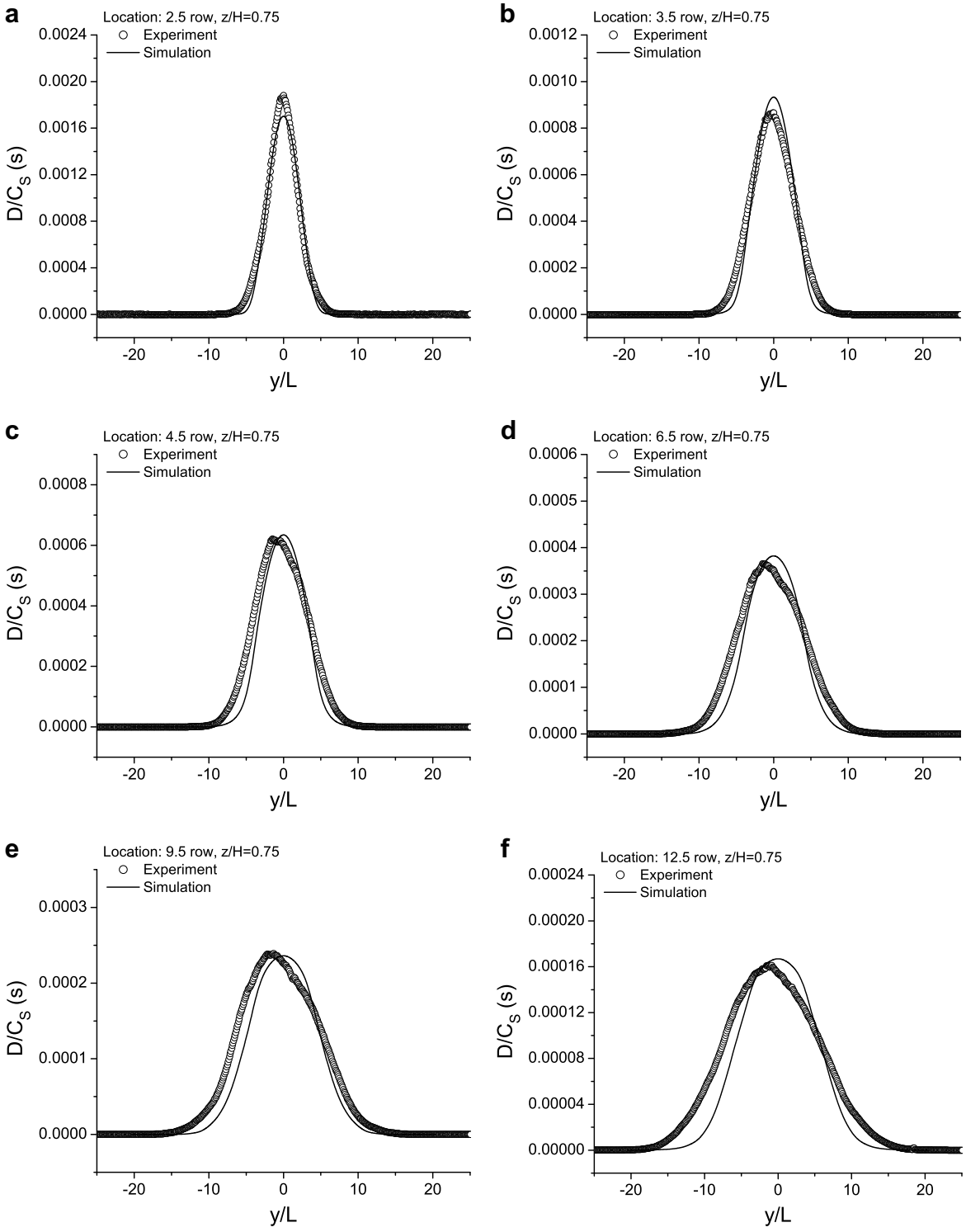

Fig. 12. Crosswind (horizontal) profiles of the total dosage $\mathscr{D}/C_s$ obtained at six x-locations within the canopy at $z/H = 0.75$. The numerical predictions were obtained using the small domain with the finer-grid resolution.

the corresponding experimental measurements. These concentration standard deviation profiles are taken along the mean cloud centerline ($y/L = 0$) at six downwind locations and at two heights, one within ($z/H = 0.75$) and one above ($z/H = 1.5$) the canopy. The numerical predictions were obtained using two different models (i.e., Model-1 and Model-2) for the dissipation length-scale, and for each of these models on both the small and large flow domains.

First, let us focus on the model predictions obtained using the closure coefficients of Yoshizawa (1985). The closure coefficients recommended by Yoshizawa (1985) are given as follows:

$$(C_{s1}, C_{s2}) = (0.134, -0.032)$$
$$(\text{Coef.-A : original coefficients of Yoshizawa (1985)}). \quad (22)$$

Coef.-A has been successfully used to compute the concentration field (first-order passive scalar moment) shown in Figs. 7 and 8

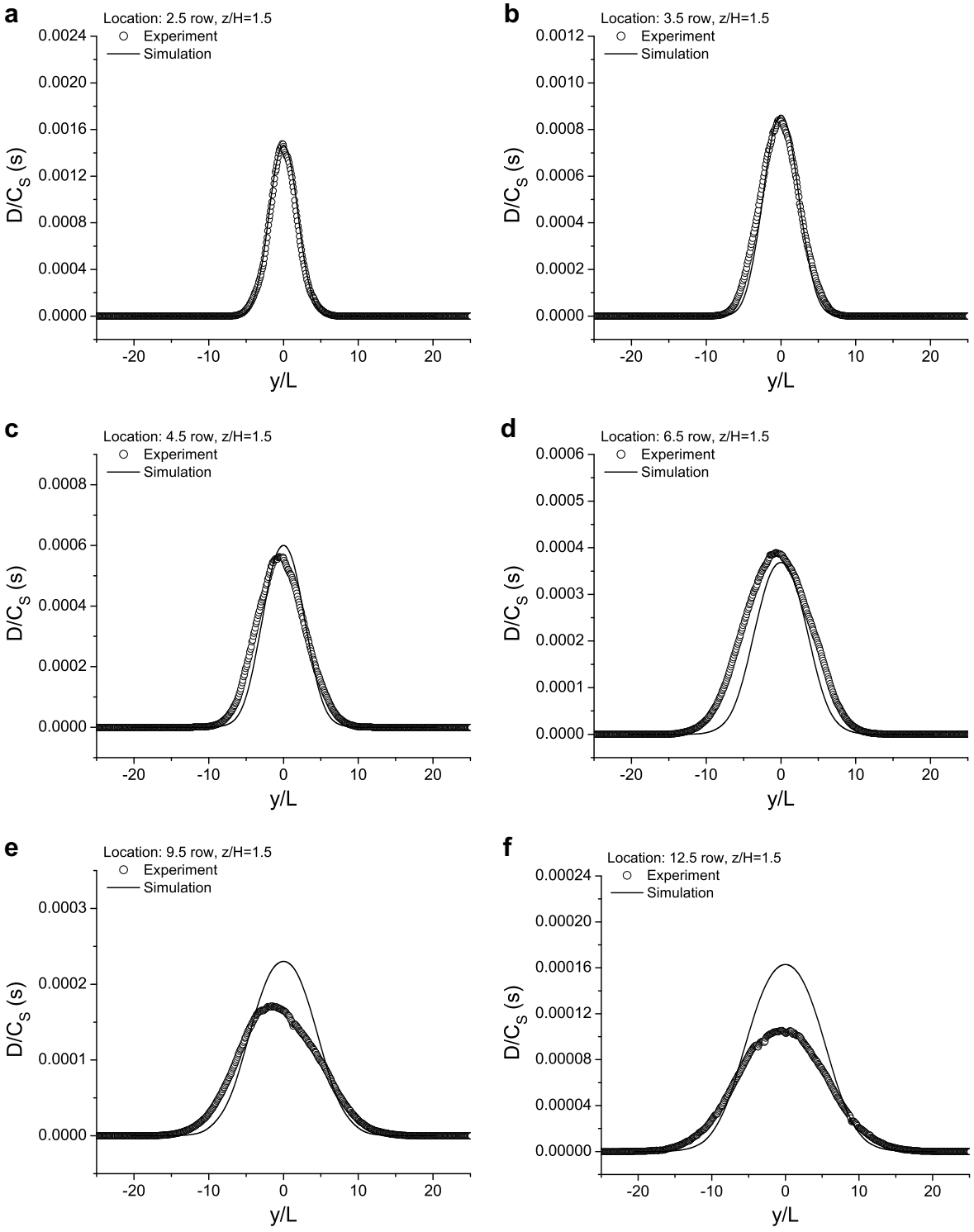

Fig. 13. Crosswind (horizontal) profiles of the total dosage $\mathscr{D}/C_s$ obtained at six x-locations above the canopy at $z/H = 1.5$. The numerical predictions were obtained using the small domain with the finer-grid resolution.

(by solving Eq. (5)). Now, it is necessary to evaluate whether this set of coefficients is also suitable for computing the concentration variance (second-order passive scalar moment) (by solving Eq. (6)). As shown in Figs. 9a and 10a, near the source (row 2.5), the prediction of the time profile of $(\overline{c'^2})^{1/2}$ obtained using Coef.-A for the turbulence scalar flux and Model-2 for the dissipation length-scale is in good conformance with the experimental data. However, further downstream from the source, the predictive accuracy for $(\overline{c'^2})^{1/2}$ deteriorates in the sense that the decay in concentration standard deviation as the cloud departs a receptor location is too slow in comparison with the experimental measurements.

This unphysical behavior in $(\overline{c'^2})^{1/2}$ can be traced back to the turbulent scalar flux model of Yoshizawa (1985). This is not too surprising owing to the fact that the current tensor diffusivity models for the turbulent scalar flux (including that of Yoshizawa) were originally designed for closure of the transport equation for

the mean concentration, rather than for the concentration variance. In view of this, we re-calibrated the closure coefficients of Yoshizawa's scalar flux model for its application to the transport equation for the concentration variance. This exercise suggests that the following set of closure coefficients should be used for Yoshizawa's model when applied for the closure of the Reynolds-averaged equation for the concentration variance:

$$(C_{s1}, C_{s2}) = (0.142, -0.012) \quad (\text{Coef.-B : modified coefficients}). \tag{23}$$

We will refer to this set of modified closure coefficients for Yoshizawa's model as Coef.-B. With reference to Figs. 9 and 10, good results are now obtained for predictions of $(\overline{c'^2})^{1/2}$ using the proposed Coef.-B, with the model profiles closely matching the experimental measurements.

Next, let us compare the performance of Model-1 and Model-2 when used in conjunction with Coef.-B. As is evident from Figs. 9c–f, Model-1 results in a significant under-prediction of $(\overline{c'^2})^{1/2}$ in the trailing portion of the cloud at locations below the canopy. Furthermore, from Figs. 10c–f, the same model combination also results in the largest over-prediction in the maximum value of $(\overline{c'^2})^{1/2}$ at locations above the canopy. Given the predictive performance of the various model combinations for the turbulent scalar flux and dissipation length-scale, it is seen that Coef.-B (for the scalar flux model) used in combination with Model-2 (for modelling the concentration variance dissipation rate) provides the best overall predictions for the concentration variance.

The total dosage is defined as the time integral of the mean concentration of the cloud:

$$\mathscr{D} = \int_0^T \bar{c} dt, \tag{24}$$

where T is a time interval chosen to be sufficiently long so as to include the entire passage of the cloud at a receptor location. Fig. 11 displays the isopleths for the total dosage in the mean cloud (normalized by C_s), in a horizontal plane through the cloud at a height of $z/H = 0.61$. Note that the passive scalar released from the ground-level point source is rapidly entrained and mixed across the width W of the obstacle in the lee recirculation zone. Owing to this rapid mixing of passive scalar in the wake region of an obstacle, there is little sensitivity of the dispersion to the scalar source location provided this location was within the recirculating wake behind the obstacle. Figs. 12 and 13 show the crosswind (horizontal) profiles of the predicted total dosage at six downwind locations at two different heights, namely at $z/H = 0.75$ and 1.5, respectively. Generally speaking, with the exception of the predictions of $\mathscr{D}$ for rows 9.5 and 12.5 at $z/H = 1.5$ (cf. Figs. 13e and f), the model predictions for $\mathscr{D}$ are in good conformance with the experimental measurements. More specifically, the crosswind dosage profiles in the array cloud are Gaussian and self-similar.

5. Conclusion

The instantaneous release of a passive tracer from a ground-level point source in the MUST array has been studied using an advanced turbulence modelling approach (viz., nonlinear model for the stress–strain relationship, tensor diffusivity (anisotropic) model for the turbulent scalar flux, and a new formulation for a scalar dissipation length-scale model). In comparison with the experimental measurements conducted in the water-channel, the RANS-based numerical simulation predicted successfully the highly disturbed mean velocity, the turbulent kinetic energy, the mean concentration and concentration variance within and above the urban canopy. In conclusion, it has been demonstrated that the modelling schemes proposed here can be used to model flow and dispersion of a passive scalar in an idealized obstacle array under the laboratory conditions considered here. Although the test results are encouraging, the modelling proposed here still needs to be further validated using other available urban flow and pollutant dispersion data from both laboratory and full-scale experiments.

In this study, Yoshizawa's (1985) tensor diffusivity model for the turbulent scalar flux was investigated for closure of the transport equations for mean concentration and concentration variance. It was demonstrated that although this model works very well for the prediction of the mean concentration field, the closure coefficients for this model needed to be re-calibrated in order for it to provide better predictions for the behavior of the concentration variance in instantaneous clouds dispersing in a built-up environment.

References

Allwine, K.J., Shinn, J.H., Streit, G.E., Clawson, K.L., Brown, M., 2002. Overview of URBAN 2000: a multiscale field study of dispersion through an urban environment. Bull. Am. Meteorol. Soc. 83, 521–536.

Allwine, K.J., Leach, M.J., Stockham, L.W., Shinn, J.S., Hosker, R.P., Bowers, J.F., Pace, J.C., 2004. Overview of Joint Urban 2003—an atmospheric dispersion study in Oklahoma City. In: Symposium on Planning, Nowcasting, and Forecasting in the Urban Zone, American Meteorological Society, Seattle, Washington, 9 pp.

Allwine, K.J., Clawson, K.L., Flaherty, J.E., Heiser, J.H., Hosker, R.P., Leach, M.J., Stockham, L.W., 2007. Urban dispersion program: urban measurements applied to emergency response. In: Seventh Symposium on the Urban Environment, American Meteorological Society, San Diego, California, 5 pp.

Andronopoulos, S., Grigoriadis, D., Robins, A., Venetsanos, A., Rafailidis, S., Bartzis, J.G., 2002. Three-dimensional modelling of concentration fluctuations in complicated geometry. Environ. Fluid Mech. 1, 415–440.

Arnold, S.J., ApSimon, H., Barlow, J., Belcher, S., Bell, M., Boddy, J.W., Britter, R., Cheng, H., Clark, R., Colvile, R.N., Dimitroulopoulou, S., Dobre, A., Greally, B., Kaur, S., Knights, A., Lawton, T., Makepeace, A., Martin, D., Neophytou, M.N., Neville, S., Nieuwenhuijsen, M., Nickless, G., Price, C., Robins, A., Shallcross, D., Simmonds, P., Smalley, R.J., Tate, J., Tomlin, A.S., Wang, H., Walsh, P., 2004. Introduction to the DAPPLE air pollution project. Sci. Total Environ. 332, 139–153.

Baik, J.-J., Kim, J.-J., 1999. A numerical study of flow and pollutant dispersion characteristics in urban street canyons. J. Appl. Meteorol. 38, 1576–1589.

Béguier, C., Dekeyser, I., Launder, B.E., 1978. Ratio of scalar and velocity dissipation time scales in shear flow turbulence. Phys. Fluids 21, 307–310.

Biltoft, C.A., 2001. Customer report for Mock Urban Setting Test, DPG Document No. WDTC-FR-01-121. Technical Report, West Desert Test Center, US Army Dugway Proving Ground, Dugway, Utah, 58 pp.

Camelli, F.E., Löhner, R., Hanna, S.R., 2004. FEFLO-URBAN CFD model evaluation of the MUST experiment. In: Buscaglia, G., Dari, E., Zamonsky, O. (Eds.), Mecánica Computational, vol. XXIII, pp. 1701–1725.

Camelli, F.E., Löhner, R., Hanna, S.R., 2005. Dispersion patterns in a heterogeneous urban area. In: Larreteguy, A. (Ed.), Mecánica Computational, vol. XXIV, pp. 1339–1354.

Coirier, W.J., Fricker, D.M., Furmanczyk, M., Kim, S., 2005. A computational fluid dynamics approach for urban area transport and dispersion modelling. Environ. Fluid Mech. 5, 443–479.

Flaherty, J.E., Lamb, B., Allwine, K.J., Allwine, E., 2007. Vertical tracer concentration profiles measured during the Joint Urban 2003 dispersion study. J. Appl. Meteorol. Climatol. 46, 2019–2037.

Gailis, R.M., Hill, A., 2006. A wind-tunnel simulation of plume dispersion within a large array of obstacles. Bound.-Lay. Meteorol. 119, 289–338.

Gatski, T.B., Speziale, C.G., 1993. On explicit algebraic stress models for complex turbulent flows. J. Fluid Mech. 254, 59–78.

Hanjalić, K., 2002. One-point closure models for buoyancy-driven turbulent flows. Annu. Rev. Fluid Mech. 34, 321–347.

Hilderman, T., Chong, R., 2007. A laboratory study of momentum and passive scalar transport and diffusion within and above a model urban canopy – final report, DRDC Document No. DRDC Suffield CR 2008-025. Technical Report, Defence R&D Canada – Suffield, Ralston, Alberta, 78 pp.

Hsieh, K.-J., Lien, F.-S., Yee, E., 2007. Numerical modelling of passive scalar dispersion in an urban canopy. J. Wind Eng. Ind. Aerodyn. 95, 1611–1636.

Kim, J.-J., Baik, J.-J., 1999. A numerical study of thermal effects on flow and pollutant dispersion in urban street canyons. J. Appl. Meteorol. 38, 1249–1261.

Launder, B.E., Spalding, D.B., 1974. The numerical computation of turbulent flows. Comput. Meth. Appl. Mech. Eng. 3, 269–289.

Leonard, B.P., 1979. A stable and accurate convective modelling procedure based on quadratic upstream interpolation. Comput. Meth. Appl. Mech. Eng. 19, 59–98.

Lien, F.-S., Leschziner, M.A., 1994a. Assessment of turbulence-transport models including non-linear RNG eddy-viscosity formulation and second-moment closure for flow over a backward-facing step. Comput. Fluids 23, 983–1004.

Lien, F.-S., Leschziner, M.A., 1994b. A general non-orthogonal collocated finite volume algorithm for turbulent flow at all speeds incorporating second-

moment turbulence-transport closure, Part 1: computational implementation. Comput. Meth. Appl. Mech. Eng. 114, 123–148.
Lien, F.-S., Leschziner, M.A., 1994c. Upstream monotonic interpolation for scalar transport with applications to complex turbulent flows. Int. J. Numer. Meth. Fluids 19, 527–548.
Liu, C.-H., Barth, M.C., 2002. Large-eddy simulation of flow and scalar transport in a modeled street canyon. J. Appl. Meteorol. 41, 660–673.
Milliez, M., Carissimo, B., 2007. Numerical simulations of pollutant dispersion in an idealized urban area, for different meteorological conditions. Bound.-Lay. Meteorol. 122, 321–342.
Milliez, M., Carissimo, B., 2008. Computational fluid dynamical modelling of concentration fluctuations in an idealized urban area. Bound.-Lay. Meteorol. 127, 241–259.
Patankar, S.V., 1980. Numerical Heat Transfer and Fluid Flow. McGraw-Hill, New York, NY.
Rhie, C.M., Chow, W.L., 1983. Numerical study of the turbulent flow past an airfoil with trailing edge separation. AIAA J. 21, 1525–1532.
Rogers, M.M., Mansour, N.N., Reynolds, W.C., 1989. An algebraic model for the turbulent flux of a passive scalar. J. Fluid Mech. 203, 77–101.
Rotach, M.W., Gryning, S.-E., Batchvarova, E., Christen, A., Vogt, R., 2004. Pollutant dispersion close to an urban surface — the BUBBLE tracer experiment. Meteorol. Atmos. Phys. 87, 39–56.
Rubinstein, R., Barton, J.M., 1991. Renormalization group analysis of anisotropic diffusion in turbulent shear flows. Phys. Fluids A 3, 415–421.
So, R.M.C., Speziale, C.G., 1999. A review of turbulent heat transfer modelling. In: Tien, C.L. (Ed.), Annual Review of Heat Transfer, vol. 10. Begell House, pp. 177–219 (Chapter 5).
So, R.M.C., Jin, L.H., Gatski, T.B., 2004. An explicit algebraic Reynolds stress and heat flux model for incompressible turbulence: Part I. Non-isothermal flow. Theor. Comput. Fluid Dyn. 17, 351–376.
Speziale, C.G., 1987. On nonlinear k–l and k–ϵ models of turbulence. J. Fluid Mech. 178, 459–475.
Stone, H.L., 1968. Iterative solution of implicit approximations of multidimensional partial differential equations. SIAM J. Numer. Anal. 5, 530–558.
Wang, B.-C., Yee, E., Lien, F.-S., 2007. Study of turbulent passive scalar dispersion within a regular array of obstacles. In: Friedrich, R., Adams, N.A., Eaton, J.K., Humphery, J.A.C., Kasagi, N., Leschziner, M.A. (Eds.), Proceedings of Fifth International Symposium on Turbulence Shear Flow Phenomena (TSFP5), Munich, Germany, pp. 797–802.
Warhaft, Z., 2000. Passive scalars in turbulent flows. Annu. Rev. Fluid Mech. 32, 203–240.
Warhaft, Z., Lumley, J.L., 1978. An experimental study of the decay of temperature fluctuations in grid-generated turbulence. J. Fluid Mech. 88, 659–684.
Warner, S., Platt, N., Heagy, J.F., Jordan, J.E., Bieberbach, G., 2006. Comparisons of transport and dispersion model predictions in the Mock Urban Setting Test field experiment. J. Appl. Meteorol. Climatol. 45, 1414–1428.
Wikström, P.M., Wallin, S., Johansson, A.V., 2000. Derivation and investigation of a new explicit algebraic model for the passive scalar flux. Phys. Fluids 12, 688–702.
Wilcox, D.C., 1998. Turbulence Modelling for CFD, second ed. DCW Industries, Inc., La Canada, California.
Yee, E., Biltoft, C.A., 2004. Concentration fluctuation measurements in a plume dispersing through a regular array of obstacles. Bound.-Lay. Meteorol. 111, 363–415.
Yee, E., Gailis, R.M., Hill, A., Hilderman, T., Kiel, D., 2006. Comparison of wind-tunnel and water-channel simulations of plume dispersion through a large array of obstacles with a scaled field experiment. Bound.-Lay. Meteorol. 121, 389–432.
Yee, E., Lien, F.-S., Ji, H., 2007. Technical description of urban microscale modelling system: component 1 of CRTI project 02-0093RD, DRDC Document No. DRDC Suffield TR 2007-067. Technical Report, Defence R&D Canada – Suffield, Ralston, Alberta, 55 pp.
Yoshizawa, A., 1985. Statistical analysis of the anisotropy of scalar diffusion in turbulent shear flows. Phys. Fluids 28, 3226–3231.
Yoshizawa, A., 1988. Statistical modelling of passive-scalar diffusion in turbulent shear flows. J. Fluid Mech. 195, 541–555.
Younis, B.A., Speziale, C.G., Clark, T.T., 2005. A rational model for the turbulent scalar fluxes. Proc. R. Soc. Lond. A 461, 575–594.